Appendix C

Energy Loss and Diffusion due to Coulomb Collisions With Warm Plasmas

C.1 Coulomb Loss in Warm Plasmas

In the previous SA model, the energy loss rate due to Coulomb collisions with the ambient plasma is calculated by assuming a cold-target scenario, in which the nonthermal electron velocity $v \gg v_{\rm th}$, where $v_{\rm th} = \sqrt{2kT/m_e}$ is the thermal velocity of the background electrons. This is a valid assumption in the high-energy regime, but it is not necessarily true for low-energy electrons whose velocity is comparable to or even less than those of the ambient electrons. In the latter case, the electrons may even gain energy from the ambient, rather than lose energy as is always the case in the cold-target scenario. More general treatment of Coulomb loss is therefore desired. Miller et al. (1996) has included such calculations in their electron acceleration model. Emslie (2003) also considered this effect when calculating particle transport and found that it can significantly reduce the inferred energy content of the injected electron distribution.

Here we briefly document how we improve on this in our current SA model. Since nonthermal electrons almost do not lose energy by collision with background protons or heavier ions, here we restrict ourselves to electron-electron collision only. The Coulomb energy loss rate for cold plasmas is:

$$\dot{E}^{\rm cold}_{\rm Coul} = 4\pi r_0^2 \ln\Lambda c n/\beta\,, \tag{C.1}$$

where $r_0 = e^2/(m_e c^2) = 2.8\times10^{-13}$ cm is the classical electron radius and $\ln\Lambda = 20$ (Leach, 1984) is a reasonable value for solar flares. Following Miller et al. (1996, eq. (2.5a))[1], we rewrite the general Coulomb loss rate (see also Benz, 2002, eq. (2.6.28); Spitzer, 1962, p. 128–129) as

$$\dot{E}_{\rm Coul} = \dot{E}^{\rm cold}_{\rm Coul}[\psi(x) - \psi'(x)], \tag{C.2}$$

[1]Note E in Miller et al. (1996) should be replaced with $\frac{1}{2}m_e v^2/(m_e c^2)$, *not* $\gamma - 1$, to make it valid in both non-relativistic and relativistic regimes, where $m_e c^2$ is used to make energy dimensionless. The same notation should be taken for Miller's eq. (2.5b); see below.

where we redefine $x = Em_ec^2/(kT)$, which is reduced to the definition of $\tilde{x} = (v/v_{\rm th})^2$ of Miller et al. (1996) at non-relativistic energies. In the relativistic regime, $x(\propto E)$ can approach ∞, which is mathematically more convenient than $\tilde{x}$ that has a finite upper limit of $(c/v_{\rm th})^2$.

$$\psi(x) = P(3/2, x) = \frac{1}{\Gamma(3/2)} \int_0^x t^{3/2-1} e^{-t} dt \tag{C.3}$$

is the incomplete gamma function (see Press et al., 1992, p. 160), where $\Gamma(a) = \int_0^\infty e^{-t} t^{a-1} dt$ is the common gamma function. Figure C.1 shows $\psi(x)$ and $\psi'(x)$, which approaches 1 and 0 very quickly, respectively, when x increases. Since

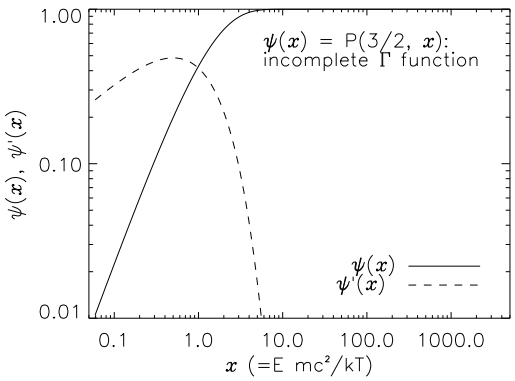

Figure C.1: Incomplete gamma function $\psi(x)$ and its derivative.

$$P(a+1, x) = P(a, x) - \frac{x^a e^{-x}}{a\Gamma(a)},$$

one can rewrite

$$\psi(x) = P(3/2, x) = P(1/2, x) - 2\sqrt{\frac{x}{\pi}} e^{-x} = \mathrm{erf}(\sqrt{x}) - 2\sqrt{\frac{x}{\pi}} e^{-x}, \tag{C.4}$$

where

$$\mathrm{erf}(\sqrt{x}) = \frac{2}{\sqrt{\pi}} \int_0^x e^{-t^2} dt \tag{C.5}$$

is the error function. One can also readily obtain

$$\psi'(x) = 2\sqrt{\frac{x}{\pi}} e^{-x}. \tag{C.6}$$

Substituting equations C.4 and C.6 to C.2, we have

$$\dot{E}_{\rm Coul} = \dot{E}^{\rm cold}_{\rm Coul} \left[\mathrm{erf}(\sqrt{x}) - 4\sqrt{\frac{x}{\pi}} e^{-x} \right], \tag{C.7}$$

in terms of more commonly used error function. The absolute value of the Coulomb loss

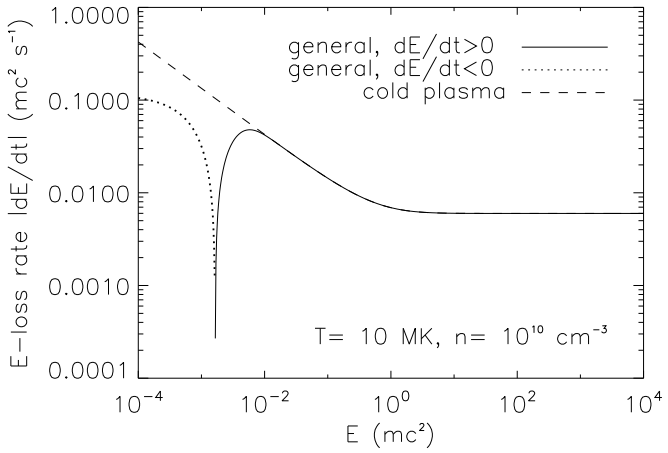

Figure C.2: Absolute value of Coulomb loss rate $\dot{E}_{\rm Coul}$ (*solid* and *dotted*) calculated for a typical background plasma condition for solar flares, $T = 10^7\,{\rm K}, n = 10^{10}\,{\rm cm}^{-3}$. Below the energy corresponding to the sharp "spike", $\dot{E}_{\rm Coul}$ turns to negative (*dotted*), meaning particle gaining energy. The cold-plasma loss rate $\dot{E}^{\rm cold}_{\rm Coul}$ (*dashed*) is shown for comparison.

rate is shown in Figure C.2, together with its counterpart of cold-target approximation. As energy decreases, this Coulomb loss rate (solid line) first increases; it then decreases and becomes negative (gaining energy). The energy at which it turns negative is very close to (but slightly less than) the thermal energy of background electrons. As expected, the cold-target Coulomb loss rate (dashed line) deviates from the general loss rate at low energies but the two agree well at high energies.

C.2 Coulomb Diffusion in Warm Plasmas

Similarly, Coulomb collision also contributes to diffusion in energy. In general, one can split the diffusion coefficient $D(E)$ into two parts:

$$D(E) = D_{\rm turb}(E) + D_{\rm Coul}(E), \tag{C.8}$$

where $D_{\rm turb}(E)$ and $D_{\rm Coul}(E)$ are contributions by turbulence and by Coulomb collisions, respectively. At low energies, energy diffusion due to Coulomb collisions becomes important, while at high energies, diffusion would be dominated by the contribution from turbulence. However, the $D_{\rm Coul}(E)$ term was not included in the previous SA mode.

Following Miller et al. (1996, eq. (2.5b))[2], we rewrite the Coulomb diffusion coefficient (see also Spitzer, 1962, p. 132)

$$D_{\rm Coul}(E) = \dot{E}^{\rm cold}_{\rm Coul}\left(\frac{kT}{m_e c^2}\right)\psi(x) = \dot{E}^{\rm cold}_{\rm Coul}\left(\frac{kT}{m_e c^2}\right)\left[{\rm erf}(\sqrt{x}) - 2\sqrt{\frac{x}{\pi}}e^{-x}\right]. \tag{C.9}$$

[2]Note $D(E)$ in eq. (C.10) here is equivalent to $D_C(E)/2$ in eq. (2.5b) of Miller et al. (1996).

C.3 Implementation of Coulomb Loss and Diffusion

The Fokker-Planck equation in some early works (Miller et al., 1996; Petrosian & Liu, 2004) was written as,

$$\frac{\partial f}{\partial t} = \frac{\partial^2}{\partial E^2}[D(E)f] - \frac{\partial}{\partial E}\{[A_1(E) - \dot{E}_{L1}]f\} - \frac{f}{T_{\rm esc}(E)} + Q(E)\,, \tag{C.10}$$

in a way which is slightly different from that of equation (1.1) used here. By substituting equation (C.8) one can rewrite this equation as

$$\frac{\partial f}{\partial t} = \frac{\partial}{\partial E}\left[D\frac{\partial f}{\partial E}\right] - \frac{\partial}{\partial E}\left\{\left[\left(A_1 - \frac{dD_{\rm turb}}{dE}\right) - \left(\dot{E}_{L1} + \frac{dD_{\rm Coul}}{dE}\right)\right] f\right\} - \frac{f}{T_{\rm esc}} + Q, \tag{C.11}$$

which can be directly compared with equation (1.1). We then identify the following relationship between the two ways of writing the Fokker-Planck equation:

$$A = A_1 - \frac{dD_{\rm turb}}{dE},^{3} \tag{C.12}$$

$$\dot{E}_L = \dot{E}_{L1} + \frac{dD_{\rm Coul}}{dE} = \dot{E}^{\rm eff}_{\rm Coul} + \dot{E}_{\rm synch}, \tag{C.13}$$

where we substitute equation (C.13) and define the effective Coulomb loss rate

$$\dot{E}^{\rm eff}_{\rm Coul} = \dot{E}_{\rm Coul} + \frac{dD_{\rm Coul}}{dE}. \tag{C.14}$$

We must modify the energy loss rate accordingly using the above two equations, when we include Coulomb diffusion using equations (C.9) and (C.8).

Let us now derive $dD_{\rm Coul}/dE$ and $\dot{E}^{\rm eff}_{\rm Coul}$. Using equation (C.9), we have

$$\frac{dD_{\rm Coul}}{dE} = D_{\rm Coul}\frac{d}{dE}\ln D_{\rm Coul} = D_{\rm Coul}\left[\frac{d}{dE}\ln \dot{E}^{\rm cold}_{\rm Coul} + \frac{d}{dE}\ln\psi(x)\right], \tag{C.15}$$

in which by equation (C.1) and $E = \gamma - 1$ we note

$$\frac{d}{dE}\ln \dot{E}^{\rm cold}_{\rm Coul} = -\frac{d\ln\beta}{dE} = -\frac{1}{\beta}\frac{d\beta}{d\gamma} = -\frac{1}{\beta^2\gamma^3} = -\frac{1}{\gamma(\gamma^2-1)} = -\frac{1}{\gamma(\gamma+1)E},$$

and by $x = Em_ec^2/kT$ we have

$$\frac{d}{dE}\ln\psi(x) = \frac{\psi'(x)}{\psi(x)}\frac{dx}{dE} = \frac{\psi'(x)}{\psi(x)}\frac{m_ec^2}{kT}.$$

Plugging the above two expressions to equation (C.15) and noting equation (C.9), we obtain

$$\frac{dD_{\rm Coul}}{dE} = \dot{E}^{\rm cold}_{\rm Coul}\left[\psi'(x) - \frac{\psi(x)}{x}\frac{1}{\gamma(\gamma+1)}\right], \tag{C.16}$$

[3] This notation conversion has already been taken care of in the code properly.

and, by using equation (C.2), the effective Coulomb loss rate

$$\dot{E}^{\rm eff}_{\rm Coul} = \dot{E}_{\rm Coul} + \frac{dD_{\rm Coul}}{dE} = \dot{E}^{\rm cold}_{\rm Coul}\psi(x)\left[1 - \frac{1}{x}\frac{1}{\gamma(\gamma+1)}\right]$$
$$= \dot{E}^{\rm cold}_{\rm Coul}\left[{\rm erf}(\sqrt{x}) - 2\sqrt{\frac{x}{\pi}}e^{-x}\right]\left[1 - \frac{1}{x}\frac{1}{\gamma(\gamma+1)}\right]. \qquad \text{(C.17)}$$

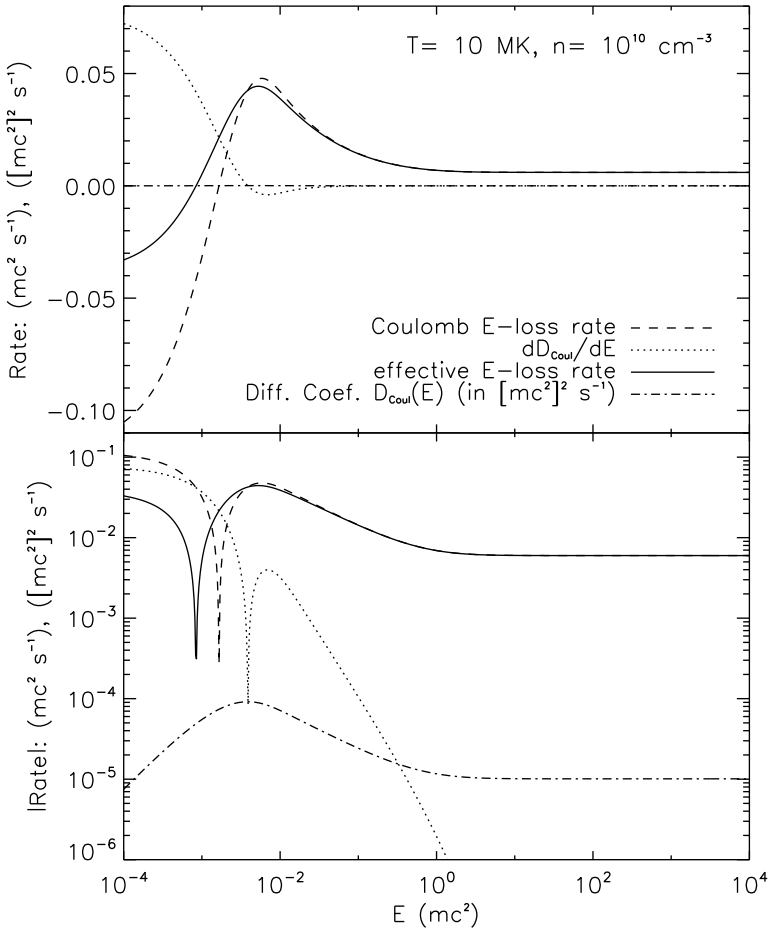

Figure C.3: Energy loss and diffusion rates due Coulomb collisions. *Top:* Coulomb energy loss rate $\dot{E}_{\rm Coul}$, diffusion coefficient $D_{\rm Coul}(E)$ and its derivative $dD_{\rm Coul}/dE$, and effective Coulomb energy loss rate $\dot{E}^{\rm eff}_{\rm Coul} = \dot{E}_{\rm Coul} + dD_{\rm Coul}/dE$. $D_{\rm Coul}(E)$ is in units of $(mc^2)^2\,{\rm s}^{-1}$ and the others are in units of $mc^2\,{\rm s}^{-1}$. *Bottom:* same as the top panel but for the absolute values plotted in a logarithmic scale.

Figure C.3 shows the energy loss or diffusion rates calculated for the same background plasma condition as in Figure C.2. As can be seen, with decreasing energy, the Coulomb energy loss rate $\dot{E}_{\rm Coul}$ changes its sign from positive to negative at about the energy of the background electron thermal energy, while the Coulomb diffusion derivative $dD_{\rm Coul}/dE$

does the opposite. The addition of the two gives the effective Coulomb loss rate $\tau_{\rm Coul}^{\rm eff}$, which is mainly dominated by $\dot{E}_{\rm Coul}$ except at low energies. The energy at which $\tau_{\rm Coul}^{\rm eff}$ flips its sign is slightly (by a half decade) lower than that of $\dot{E}_{\rm Coul}$.

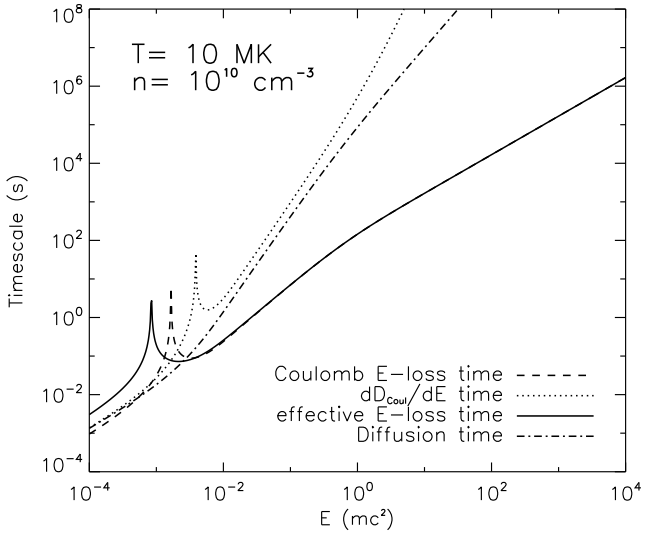

Figure C.4: Coulomb loss and diffusion timescales: $\tau_{\rm Coul}$, $\tau_{D'_{\rm Coul}}$, $\tau_{\rm Coul}^{\rm eff}(=[1/\tau_{\rm Coul}+1/\tau_{D'_{\rm Coul}}]^{-1})$, and $\tau_{D_{\rm Coul}}$ (see text for definitions), corresponding to the rates plotted in Fig. C.3. Note the spikes indicate infinite time and are located at the energy where the corresponding rate changes its sign (i.e., the rate equals zero). See the top panel of Fig. C.3 for their signs.

It is convenient to define various timescales based on the above obtained coefficients:

$$\tau_{\rm Coul}^{\rm cold} = E/\dot{E}_{\rm Coul}^{\rm cold} = (\gamma-1)\beta(4\pi r_0^2 \ln\Lambda cn)^{-1}, \tag{C.18}$$

$$\tau_{\rm Coul} = E/|\dot{E}_{\rm Coul}| = \tau_{\rm Coul}^{\rm cold}|\psi(x)-\psi'(x)|^{-1}, \tag{C.19}$$

$$\tau_{\rm Coul}^{\rm eff} = E/|\dot{E}_{\rm Coul}^{\rm eff}| = \tau_{\rm Coul}^{\rm cold}\left|1-\frac{1}{x}\frac{1}{\gamma(\gamma+1)}\right|^{-1}/|\psi(x)|, \tag{C.20}$$

$$\tau_{D'_{\rm Coul}} = \frac{E}{|dD_{\rm Coul}/dE|} = \tau_{\rm Coul}^{\rm cold}\left|\psi'(x)-\frac{\psi(x)}{x}\frac{1}{\gamma(\gamma+1)}\right|^{-1}, \tag{C.21}$$

$$\tau_{D_{\rm Coul}} = E^2/D_{\rm Coul} = E^2[\dot{E}_{\rm Coul}^{\rm cold}(kT/m_ec^2)\psi(x)]^{-1} = \tau_{\rm Coul}^{\rm cold}x/\psi(x), \tag{C.22}$$

Figure C.4 shows these timescales, which is proportional to the inverse of the bottom panel of Figure C.3. We note that above $\sim$ 10 keV (about 10 times higher than the thermal energy of background electrons), both Coulomb diffusion time and the $dD_{\rm Coul}/dE$ time are sufficiently large that Coulomb diffusion can be neglected in the Fokker-Planck calculation, as the previous SA model does.

C.4 Thermalization Test of Injected Distribution

We have tested the implementation of the new Coulomb loss and diffusion. We turned off acceleration by turbulence, but left Coulomb loss and diffusion on in the code. We injected a narrow Gaussian (δ-function like) distribution of electrons with a mean energy of 1 keV into a background plasma of Maxwellian distribution with a temperature of 1 keV and a density of $n_e = 1.5 \times 10^{10}\,\mathrm{cm}^{-3}$. We then calculated the time-dependent spectrum of these electrons. Figure C.5 shows the evolution of the electron distribution in separate time intervals (*left*: 0–0.01 s, *middle*: 0.01–0.1 s, *right*: 0.1-1 s). The injected Gaussian (*black*) and the background Maxwellian (*gray*) distribution are plotted in all the panels as a reference. As can be seen, the distribution quickly thermalizes and approaches the background Maxwellian distribution (overlapping with the final distribution at $t = 1\,\mathrm{s}$). From Figure C.4, we note that the Coulomb diffusion timescale $\tau_{D_{\mathrm{Coul}}}$ is about 0.1 s at $E = 1\,\mathrm{keV}$ in a plasma of $n_e = 1 \times 10^{10}\,\mathrm{cm}^{-3}$ (similar to the density here). The duration of 1 s in this calculation is thus about 10 times longer than the diffusion timescale, which allows sufficient time for the thermalization to happen.

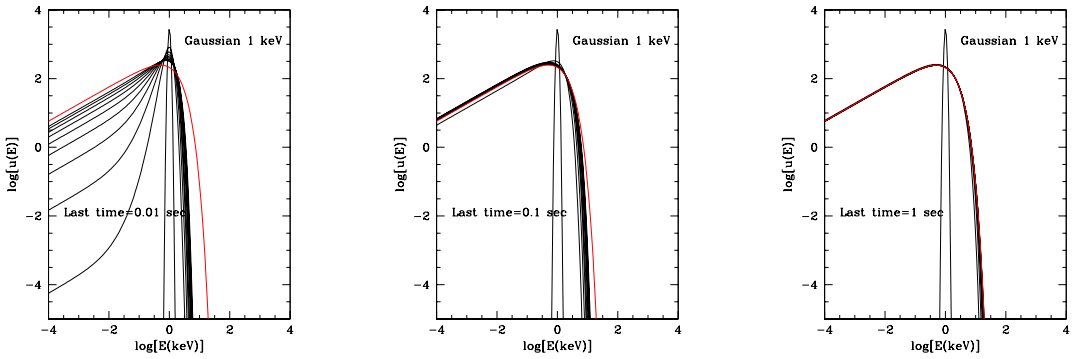

Figure C.5: Test against thermal distribution for injected Gaussian distribution when Coulomb diffusion is included. The injected narrow Gaussian (*black*) and the background Maxwellian (*gray scale*) distributions are fixed in each panel as a reference. The other curves (*black*, evenly spaced in time) in each panel show the temporal evolution on different stages *left*: 0–0.01 s, *middle*: 0.01–0.1 s, *right*: 0.1-1 s [Courtesy of William East].